Phasor-domain Dynamic Model of Asymmetric Current Injection Controller for Converter-interfaced Generator

Victor A. F. Almeida, Glauco N. Taranto, and José M. T. Marinho

***Abstract*—This paper presents a controller model of asymmetric current injection for converter-interfaced generators suitable for root-mean-square (RMS) phasor-domain, fundamental-frequency, three-phase, and dynamic simulation tools. The effectiveness of the proposed controller is assessed with simulations in test systems with high percentage of converter-interfaced generation. The simulations focus on the operation of protection relays that use negative-sequence quantities in their directional elements. This paper also presents and compares two strategies to limit reactive negative-sequence currents, and active and reactive positive-sequence currents. A tutorial test system and a regional system part of the actual Brazilian Interconnected Power System are used to assess the correctness of the proposed controller in three-phase fundamental-frequency RMS dynamic simulations.**

***Index Terms*—Converter-interfaced generator, three-phase model, power system protection, negative-sequence current injection, negative-sequence current protection, unbalanced fault, three-phase root-mean-square (RMS) dynamic simulation.**

I. Introduction

With the increasing pressure on environmental concerns, many countries are going through a process of reducing the utilization of conventional fossil fuel generation. In addition to this trend, technological advances and cost reduction in solar and wind sources have made a conductive environment for a fast-paced penetration of converter-interfaced generators (CIGs) in the bulk power system (BPS).

Due to the specific electrical characteristics introduced by the CIG, increasing challenges arise so that the BPS remains functional. Besides important issues like the relative reduction of synchronous rotating inertia, an increasingly noticed effect due to the presence of CIG is the reduction of short-circuit capacity in the system [1], [2]. Unlike CIGs, conventional synchronous generators (SGs) can provide high inductive short-circuit currents during a fault. This principle is of paramount importance in setting protection relays, while differentiating fault from normal operating conditions. CIGs do not have the ability to inject high currents due to the limiting overload capability of power electronics switches (normally, 10%-30% above the rated current). In addition, these sources normally do not inject negative- or zero-sequence currents during asymmetric faults. This fact can cause protection malfunctioning on the directional function of distance relays relying on negative-sequence quantities.

Several works [3]-[6] in the area of power system dynamics, protection, and control deal with the use of negative-sequence quantities for protections. The use of asymmetric sequences for protection in the BPS is very useful because the negative and zero sequences are negligible in the normal operation (unless small unbalances). Therefore, there is a large headroom for setting the relay pickup values. Reference [7] presents the electrical characteristics of a generating source connected through a full-scale converter. The electrical impacts of the decoupling of these systems due to the rectifier and inverter bridges and how the control of these power electronics switches impacts the short-circuit currents are discussed. These are important fundamental concepts that help obtain the full understanding of this paper. Reference [7] also presents the inverter mode control that suppresses the negative-sequence current and its consequences. The suppression of negative-sequence current is the main factor that changes the behavior of the CIG compared with the SGs in the short-circuit contribution under unbalanced faults. It causes a reduction in the magnitude of the negative-sequence current, as well as the problems for the directionality of the relays that use negative sequence. The suppression of negative-sequence current causes the impedance of the negative-sequence circuit of the inverter to be very high.

References [8]-[11] highlight the impact of CIGs on the protection of electrical systems, especially on overcurrent and distance relays, and their directional elements. Unlike the behavior of SGs under asymmetrical faults, the CIG control mode of injecting only positive-sequence currents can dramatically change the relationship between negative-sequence voltage and current, possibly causing the protection to fail. This protection problem has been early identified,

Manuscript received: June 26, 2021; accepted: November 2, 2021. Date of CrossCheck: November 2, 2021. Date of online publication: November 30, 2021.

This work was supported by CNPQ, FAPERJ and Coordenação de Aperfeiçoamento de Pessoal de Nível Superior – Brasil (CAPES) Finance Code 001.

V. A. F. Almeida (corresponding author) and G. N. Taranto are with the Electrical Engineering Department of the Federal University of Rio de Janeiro (COPPE/UFRJ), Rio de Janeiro, RJ, Brazil (e-mail: victor_freitas@poli.ufrj.br; glaucotaranto@coppe.ufrj.br).

J. M. T. Marinho is with Petrobras S. A., Rio de Janeiro, RJ, Brazil (e-mail: jmtmarinho@petrobras.com.br).

DOI: 10.35833/MPCE.2021.000407

and [12] - [16] present strategies for injecting negative-sequence current under asymmetrical faults. The main difference presented by the previous works and this paper is that the previous works focus on electromechanical dynamic (EMT) simulations of small-scale equivalent systems, while this paper focuses on three-phase root-mean-square (TP-RMS) dynamic simulations of interconnection-wide systems in fundamental frequency.

Currently, the German code VDE-AR-N 4130 [17] requires the injection of negative-sequence current to avoid the aforementioned protection problems. Reference [2] also comments on the German code, stating that asymmetrical injections should occur when identifying negative-sequence voltages at the converter terminal of CIG grid.

The asymmetric current injection controller of CIG proposed in this paper is modeled in three-phase fundamental-frequency phasor domain for EMT simulation [18]. The TP-RMS dynamic simulation model has some advantages compared with the more conventional positive-sequence RMS (PS-RMS) dynamic simulation and the steady-state short-circuit models, as it can represent relays involved in neutral/ground circuitry, while capturing the system dynamics. It makes it possible to gauge the functioning of relays that use negative- and zero-sequence quantities and design of equipment control under load imbalances or asymmetric faults. Despite being computationally heavier than PS-RMS simulation, it is much faster than EMT tools for interconnection-wide simulations. This paper goes along the line of [18], which promotes the integration of relay models in TP-RMS simulation and their applications in large-scale systems, where the computational burden of EMT model is prohibitive.

Like [12], this paper also presents and compares two proposals to limit the reactive negative-sequence currents, and active and reactive positive-sequence currents. A tutorial test system and a regional system part of the actual Brazilian Interconnected Power System (BIPS) are considered to assess the correctness of the proposed controller in TP-RMS dynamic simulations.

II. TP-RMS Dynamic Model of Generator Connected Through Full-scale Converter

The CIG dynamic model used in this paper is based on the generic Western Electricity Coordinating Council (WECC) models presented in [19] and [20] for wind and photovoltaic (PV) generation, respectively. The difference lies in the three-phase representation of the models [21] utilized in this paper.

The present dynamic model is aimed at analyzing electromechanical problems in the electrical network, disregarding the fast-switching converter dynamics. Despite being more accurate, the EMT models still have a prohibitive computational burden for interconnection-wide simulation studies.

Figure 1 shows the simplified block diagram of the WECC-based three-phase CIG dynamic model. A controlled source, given by the modules Renewable Energy Generator/Converter (REGC), Renewable Energy Electrical Control (REEC), and Renewable Energy Plant-level Control (REPC), injects a positive-sequence current into the terminal bus. Without negative- and zero-sequence current injections, these two sequences have a zero-magnitude zero-angle controlled source. The three-phase model can indirectly inject asymmetrical currents by an uncontrolled impedance shunt source coming from the Norton equivalent circuit.

The generating plant receives the voltage V_{reg} and frequency F_{reg} signals to be controlled based on the voltage V_{ref} and frequency F_{ref} or on the active and reactive power references P_{ref} and Q_{ref}, respectively. The resulting power signals P_{ext} and Q_{ext} are processed into the auxiliary active and reactive current signals I'_{pcmd} and I'_{qcmd}, respectively. These signals pass through a current limiter that generates I_{pcmd} and I_{qcmd}. Finally, the generator control injects the positive-sequence current I_1.

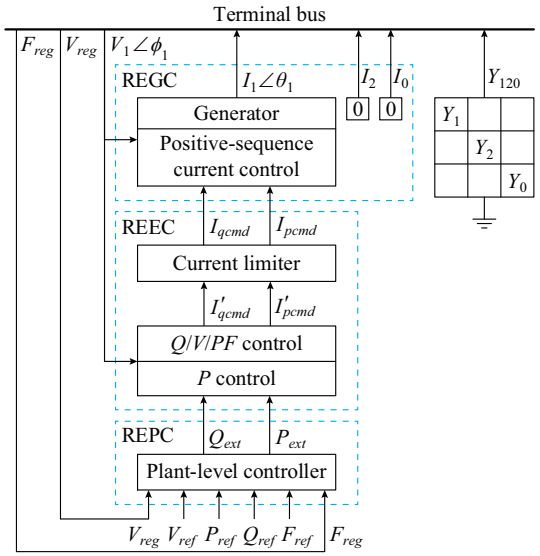

Fig. 1. Block diagram of three-phase model for concentrated PV generator.

For the uncontrolled shunt impedance source, Y_1 is null because the behavior of the generating source connected through a full-scale converter in the positive sequence is given by an ideal controlled current source (infinite internal impedance), with control regulation at the bus connected to CIG terminal or at a remote bus. The zero-sequence admittance Y_0, is null as the inverters are usually built in a 3-legged bridge. Thus, there is no path to the zero-sequence current. Finally, Y_2 depends on the manufacturer philosophy, which may or may not have an ideal zero value.

III. Negative-sequence Current Control of CIGs

The negative-sequence impedance of the CIG sources is high, which is the major difference between the CIG and the conventional generating sources that causes different angular relationships between the negative-sequence current and voltage. In SGs, the negative-sequence impedance is predominantly inductive, causing the current supplied by this negative-sequence source to be approximately 90° ahead of the negative-sequence voltage. In the case of CIG, the negative-sequence current can be zero or have a resistive, inductive, or capacitive behavior, depending on the inverter controls.

Figure 2 shows the schematic diagram of a tutorial system with two generators, one of which connected to bus 1 is a CIG, and the other one connected to bus 5 is a conventional SG. A single-phase-to-ground short circuit is applied to TL2 at a distance x from the terminal of bus 3. In the representation of positive, negative, and zero sequences, the negative current $I_{2,CIG}$ and the negative impedance $Z_{2,CIG}$ are variables depending on the inverter control. In general, $I_{2,CIG}=0$ and $Z_{2,CIG}\to\infty$, providing no negative-sequence current to the fault. Transmission lines (TLs) are modeled as a PI model, but for the sake of clarity, their shunt capacitances are omitted in Fig. 2.

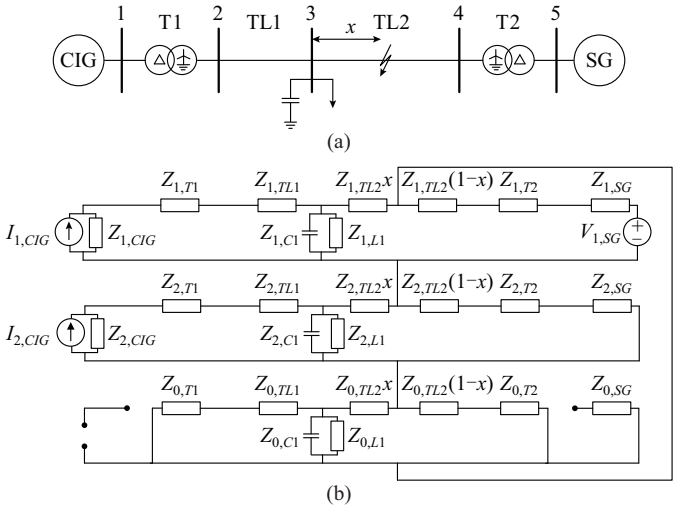

Fig. 2. Single-phase short circuit on a TL connecting PV systems with SG. (a) Topology. (b) Equivalent model.

The strategy of injecting negative-sequence currents follows some principles adopted in [12]-[16]. Reactive negative-sequence currents are injected through the detection of a negative-sequence voltage at the converter's terminal, which may indicate the existence of an asymmetric fault in the network. A dead band is required to avoid injecting negative-sequence current during normal system operation such as load unbalances. The slope of the negative-sequence current injection line is defined by parameter K_{neg}. Figure 3 presents this philosophy of injecting negative-sequence currents.

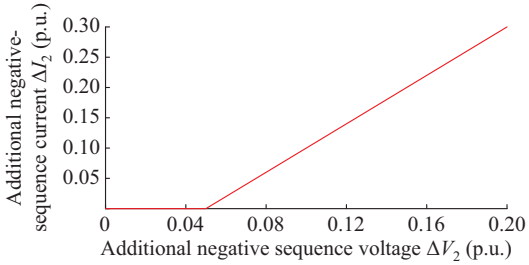

Fig. 3. Negative-sequence current injection strategy.

In the adopted three-phase RMS dynamic model, the injection of negative-sequence currents can be done by the Norton equivalent circuit either through the negative-sequence current injection source, or through the change of the negative-sequence shunt admittance. In this paper, we choose to change the negative-sequence current source I_2. Thus, the shunt admittance Y_2 is equal to zero. The negative-sequence reference current is given so that it is 90° ahead of the negative-sequence voltage, according to (1). Manipulating the exponential in (1), it is possible to obtain the expressions for the real and imaginary parts of phasor $\dot{I}_2$, given by (2) and (3), respectively. With the injection of negative-sequence currents, the block diagram of Fig. 1 is expanded into the block diagram shown in Fig. 4.

$$\dot{I}_2 = \mathrm{j}K_{neg}\left(V_2 - V_{ddbd}\right)\exp\left(\mathrm{j}\phi_2\right) \tag{1}$$

$$\mathrm{Re}\left\{\dot{I}_2\right\} = -K_{neg}\left(V_2 - V_{ddbd}\right)\mathrm{Im}\left\{\dot{V}_2\right\}/V_2 \tag{2}$$

$$\mathrm{Im}\left\{\dot{I}_2\right\} = K_{neg}\left(V_2 - V_{ddbd}\right)\mathrm{Re}\left\{\dot{V}_2\right\}/V_2 \tag{3}$$

where V_2 is the magnitude of the negative-sequence voltage phasor $\dot{V}_2$ at the terminal bus of inverter; ϕ_2 is the phase of $\dot{V}_2$; and V_{ddbd} is the dead band shown in Fig. 3, having the value of 0.05 p.u.. The negative-sequence control provides a current signal I'_{2cmd} from the negative-sequence voltage at the converter terminal. This signal is limited due to the current-carrying capability of the converter for a command current I_{2cmd}. This signal passes through the generator control, which has the negative-sequence current I_2 as its output variable.

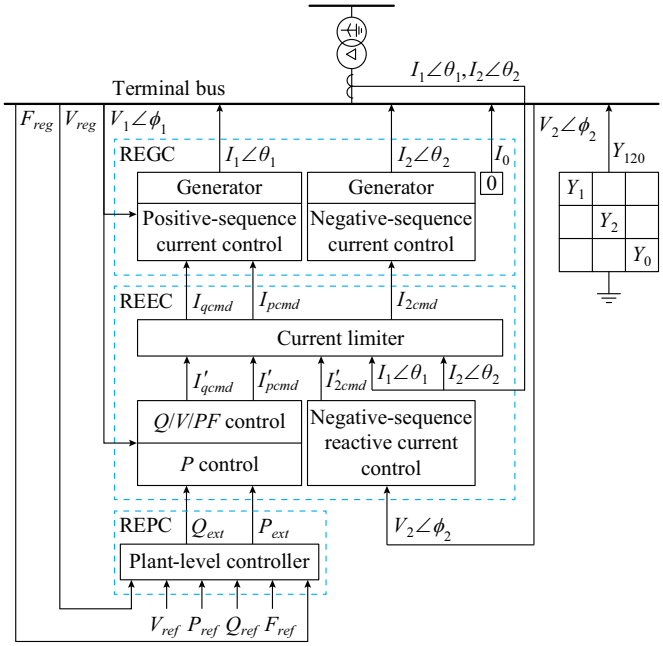

Fig. 4. Block diagram of three-phase model for PV generator with negative-sequence current injection.

Figure 5 shows the block diagram of the negative-sequence reference current I_{2ref} partially based on [12]. The negative-sequence voltage signal V_2 must pass through a sequence filter block becoming V_{2fltr}. From there, it follows the philosophy given in Fig. 3. The lead-lag block in Fig. 5, together with the proportional-integral (PI) blocks in Fig. 6, has the control parameters to modulate the system response. Figure 6 shows the block diagram of real and imaginary parts of the negative-sequence current injection based on (2) and (3), respectively. The reference signal I_{2ref} is separated

into real part $I_{2rreref}$ and imaginary part I_{2imref}. These reference signals are processed by non-windup PI blocks, which limits the signals I'_{2recmd} and I'_{2imcmd} to I_{2recmd} and I_{2imcmd}, respectively. The first-order blocks with time constant T_g models the inverter in the RMS framework, which generates I_{2re} and I_{2im}, the real and imaginary parts of negative-sequence current I_2, respectively.

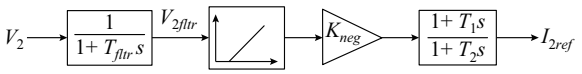

Fig. 5. Block diagram of generating negative-sequence reference current.

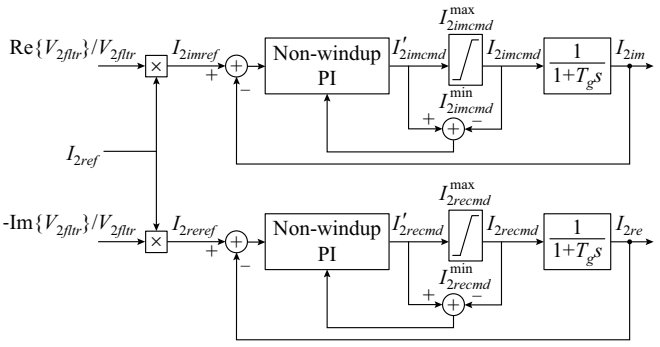

Fig. 6. Block diagram of generating real and imaginary parts of negative-sequence current.

From the block diagram, some relationships can be explained through (4)-(9). They define the relationships of the dynamic limits $I^{\max}_{2recmd}$, $I^{\min}_{2recmd}$, $I^{\max}_{2imcmd}$, and $I^{\min}_{2imcmd}$, the maximum and minimum limits of real and imaginary negative-sequence current command, respectively, in relation to the limit $I^{\max}_{2cmd}$. These limiters restrict the auxiliary command current I'_{2cmd} to the command current I_{2cmd}.

$$I_{2cmd}=\sqrt{I^2_{2recmd}+I^2_{2imcmd}} \tag{4}$$

$$I'_{2cmd}=\sqrt{\left(I'_{2recmd}\right)^2+\left(I'_{2imcmd}\right)^2} \tag{5}$$

$$I^{\max}_{2recmd}=I^{\max}_{2cmd}\left|\cos\left(\arctan\left(I'_{2imcmd}/I'_{2recmd}\right)\right)\right| \tag{6}$$

$$I^{\max}_{2recmd}=-I^{\min}_{2recmd} \tag{7}$$

$$I^{\max}_{2imcmd}=I^{\max}_{2cmd}\left|\sin\left(\arctan\left(I'_{2imcmd}/I'_{2recmd}\right)\right)\right| \tag{8}$$

$$I^{\max}_{2imcmd}=-I^{\min}_{2imcmd} \tag{9}$$

The current limitation strategy is extremely important when it comes to CIGs. The inverters are not capable of supplying currents well above their nominal values, ranging normally from 1.1 p.u. to 1.3 p.u.. The injection of negative-sequence current I_2 constrains the ability of supplying positive-sequence current I_1. Because of that, it is important to define the current injection priorities. In the same way that the generic WECC model is extended to its three-phase counterpart model, the current priorities of the three-phase symmetrical injection model (PQ priority), can be further extended to take into account the injection of negative-sequence currents (NQP priority). NQP priority gives the first priority to the negative-sequence current (N), the second priority to the reactive positive-sequence current (Q), and the last priority to the active positive-sequence current (P), and similarly, for the other priorities. Two forms of current limitation are available in the literature. A simplified limitation strategy that reflects the most restrictive condition of the relationship between negative- and positive-sequence currents are defined by (10) or (11).

$$\left|I_1\right|+\left|I_2\right|\le I^{\max} \tag{10}$$

$$\sqrt{I_p^2+I_q^2}+I_2\le I^{\max} \tag{11}$$

where I_p and I_q are the active and reactive positive-sequence currents, respectively. From this simplified expression, six possible priorities (NQP, NPQ, QNP, QPN, PNQ and PQN) can be defined with respect to $I^{\max}$, the negative-sequence command current I_{2cmd} and the positive-sequence command currents I_{pcmd} and I_{qcmd}, defining their maximum values $I^{\max}_{2cmd}$, $I^{\max}_{pcmd}$, and $I^{\max}_{qcmd}$, respectively. Three of these priorities, NQP, QNP, and PQN, are presented in (12)-(14), respectively.

$$\begin{cases} I^{\max}_{2cmd}=I^{\max} \\ I^{\max}_{qcmd}=I^{\max}-\left|I_{2cmd}\right| \\ I^{\max}_{pcmd}=\sqrt{\left(I^{\max}-I_{2cmd}\right)^2-I^2_{qcmd}} \end{cases} \tag{12}$$

$$\begin{cases} I^{\max}_{qcmd}=I^{\max} \\ I^{\max}_{2cmd}=I^{\max}-\left|I_{qcmd}\right| \\ I^{\max}_{pcmd}=\sqrt{\left(I^{\max}-I_{2cmd}\right)^2-I^2_{qcmd}} \end{cases} \tag{13}$$

$$\begin{cases} I^{\max}_{pcmd}=I^{\max} \\ I^{\max}_{qcmd}=\sqrt{\left(I^{\max}\right)^2-I^2_{qcmd}} \\ I^{\max}_{2cmd}=I^{\max}-\sqrt{I^2_{pcmd}+I^2_{qcmd}} \end{cases} \tag{14}$$

The other current limitation strategy that uses the entire current capacity of the inverter is based on [22], and will be referred to as complete limitation strategy, which is expressed in (15) and (16).

$$\alpha=\theta_2-\theta_1 \tag{15}$$

$$\sqrt{I_1^2+I_2^2+2I_1I_2\cos\left(\alpha+4\pi k/3\right)}\le I^{\max} \tag{16}$$

where k can be 0, 1, or –1, for phases a, b, and c, respectively; θ_1 is the positive-sequence current angle; and θ_2 is the negative-sequence current angle.

With this limitation, it is possible to obtain a gain of up to 15% if the difference between the angles of the injected negative- and positive-sequence currents are 60°, 180°, 300°, etc. For each α value, a corresponding k is presented in (17). Similar to the previous current limitation strategy, six priorities can be constructed from (16).

$$k=\begin{cases} -1 & -\pi\le\alpha<-\pi/3 \\ 0 & -\pi/3\le\alpha<\pi/3 \\ 1 & \pi/3\le\alpha<\pi \end{cases} \tag{17}$$

IV. Relay Model

In this paper, a multifunction relay model containing

ANSI 21 (distance function) and ANSI 67Q (negative-sequence directional overcurrent function) is used, as shown in Fig. 7. In this relay, the measured quantities are obtained through a current transformer (CT) and a potential transformer (PT). The CT measures the current phasors of each phase, and the PT measures the voltage phasors of each phase, from which we compute the negative-sequence current and voltage phasors, respectively. For the relay operation, at least one of the six fault loops (AG, BG, CG, AB, BC, and CA) must be sensitized and the fault must be declared as a forward fault by the 67Q element. Even if the impedance of any of the loops is within the protection zone, the relay will not operate, if the 67Q element (which supervises the 21 element) declares the fault as a reverse fault.

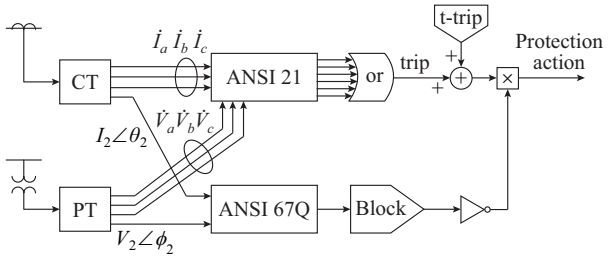

Fig. 7. Multifunction relay containing ANSI 21 and ANSI 67Q.

V. Simulation Results

A. Tutorial Test System

We perform the first TP-RMS simulations in the test system depicted in Fig. 2. Cases are generated, in which the generator at bus 1 is either an SG or a concentrated PV plant with local voltage control and over-frequency plant-level control. In the steady state, the generator at bus 1 provides 50 MW at unity power factor. The nominal capacity of this plant is assumed to be 55 MVA. Bus 3 has a load of 100 MW with an inductive power factor of 0.95, and a capacitor bank. The generator at bus 5 is a conventional SG. In the case of a concentrated PV plant, the maximum current of the inverter is assumed to be 1.2 p.u.. A single-phase-to-ground fault (phase A) in the middle of TL2 is applied for 100 ms. This TL has multifunction relays, as shown in Fig. 7, at its two terminals with 50 ms of operation time. In the TP-RMS simulations, the relay is configured in monitoring mode, that is, it informs whether the relay would operate or not, but does not trip the circuit breaker.

1) Sensitivity of Parameter K_{neg}

The first simulation compares the results of a conventional SG, a CIG with negative-sequence current (I_2) suppression, and a CIG with negative-sequence current injection control with NQP priority (simplified limitation strategy) when $K_{neg} = 2, 4, 6$.

Figure 8 shows the negative-sequence current of the generator at bus 1. It is observed that the SG has a current injection above 0.5 p.u., in contrast to the CIG with negative-sequence current suppression. As the parameter K_{neg} increases, there is an increase in the negative-sequence current injected by the CIG. Figure 9 shows the negative-sequence voltage at bus 1. As the negative-sequence current of generator at bus 1 increases, by augmenting K_{neg}, there is a reduction in the negative-sequence voltage.

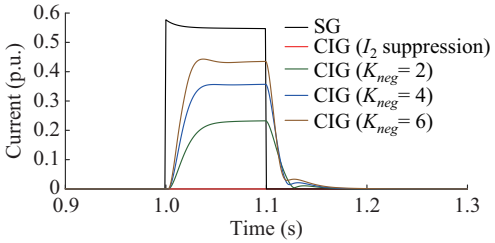

Fig. 8. Negative-sequence current of generator at bus 1.

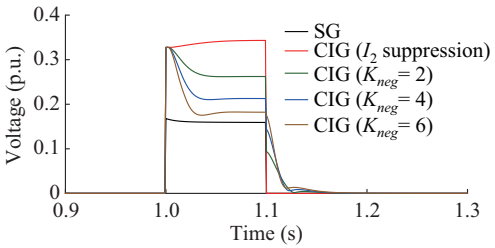

Fig. 9. Negative-sequence voltage at bus 1.

Figure 10 shows the negative-sequence current of TL2 at the terminal of bus 3. It is observed that, in this case, the level of negative-sequence current with SG is higher than that with CIG. As K_{neg} increases, there is first a reduction in the current level due to the predominance of the negative-sequence voltage reduction dynamics, which reduces the currents through the load, the capacitor bank, and the TL PI-model shunts. However, as K_{neg} increases further, the negative-sequence current of TL2 also increases.

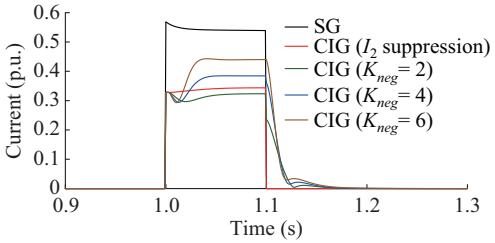

Fig. 10. Negative-sequence current of TL2 at terminal of bus 3.

Finally, Fig. 11 shows the angular difference between the negative-sequence current and voltage of TL2 at the terminal of bus 3. It is observed that, in the case of SG, the current leads the voltage by 120°. In the case of negative-sequence current suppression, the current leads the voltage by 198° (lag the voltage by 162°). As K_{neg} increases, the current returns to lead the voltage, with a behavior similar to that of a SG.

In this simulation, the relay on TL2 at the terminal of bus 4 would have been operated. However, the relay on TL2 at the terminal of bus 3 would not operate in the case of negative-sequence current suppression, as shown in Table I. In the case of negative-sequence current suppression, the ANSI 67Q detects a reverse fault due to unfavorable angular relationship between negative-sequence quantities, thus causing a protection misoperation.

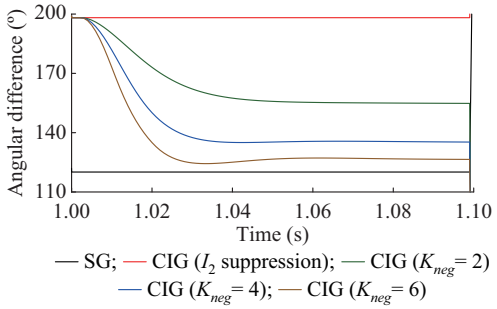

Fig. 11. Angular difference between negative-sequence current and voltage of TL2 at terminal of bus 3.

TABLE I
RELAY OPERATION ON TL2 AT TERMINAL OF BUS 3

Case	ANSI 21	Directionality of ANSI 67Q
SG	Sensitized	Forward
CIG (I_2 suppression)	Sensitized	Reverse
CIG (K_{neg} = 2)	Sensitized	Forward
CIG (K_{neg} = 4)	Sensitized	Forward
CIG (K_{neg} = 6)	Sensitized	Forward

2) Current Priority Sensitivity

A second control sensitivity analysis refers to the current limitation. The same event as in the previous case, with K_{neg} = 5, is tested on the six different priorities with the simplified limitation strategy. The priorities NPQ, QPN, and PNQ, not explicitly given in this paper, can be readily deduced.

Figure 12 shows the negative-sequence currents injected from generator at bus 1 with different priorities. It is observed that the NQP and NPQ priorities have the largest injected negative-sequence currents. The QNP priority also injects a significant amount of negative-sequence current. As expected, the QPN, PQN, and PNQ priorities do not inject significant amounts of negative-sequence currents.

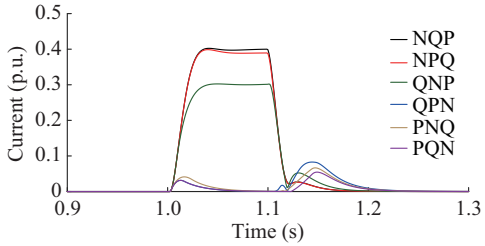

Fig. 12. Negative-sequence current of generator at bus 1 with different priorities.

Figure 13 shows the positive-sequence voltage at bus 1. It is observed that, compared with the cases where the reactive positive-sequence current has the highest priority (QNP and QPN), the NPQ and NQP cases have a lower voltage support in positive sequence due to the converter current limitation.

Finally, Fig. 14 shows the angular difference between the negative-sequence current and voltage of TL2 at the terminal of bus 3 with six priorities. As summarized in Table II, it is noted that the relay on TL2 at the terminal of bus 3 would operate only with NQP, NPQ, and QNP priorities. The other three priorities do not inject enough negative-sequence currents to adjust the angular difference in the current and voltage quantities, causing the ANSI 67Q to declare the fault as reverse in these priorities, which causes the relay not to operate.

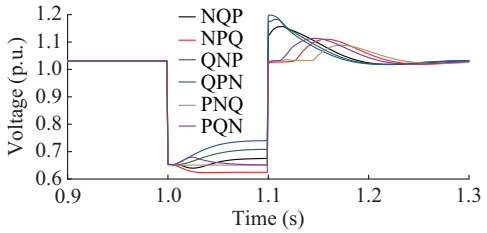

Fig. 13. Positive-sequence voltage at bus 1 with different priorities.

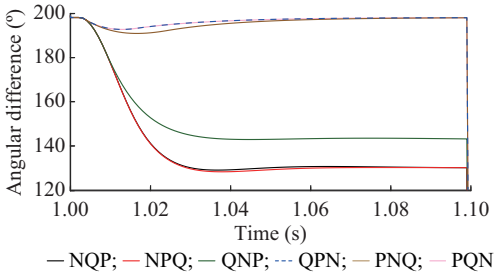

Fig. 14. Angular difference between negative-sequence current and voltage of TL2 at terminal of bus 3 with different priorities.

TABLE II
SIMULATION RELAY OPERATION ON TL2 AT TERMINAL OF BUS 3 WITH DIFFERENT PRIORITIES

Priority	ANSI 21	Directionality of ANSI 67Q
NQP	Sensitized	Forward
NPQ	Sensitized	Forward
QNP	Sensitized	Forward
QPN	Sensitized	Reverse
PQN	Sensitized	Reverse
PNQ	Sensitized	Reverse

3) Current Limitation Strategy

A third sensitivity analysis refers to the use of the simplified strategy ((10) and (11)) and complete current limitation model (16). For the sake of brevity, only the NQP priority is presented for comparison. Figure 15 shows the negative-sequence current injected from generator at bus 1 with the two limitation strategies. Figure 16 shows the positive-sequence voltage at bus 1, and Fig. 17 shows the active power output of generator at bus 1. It is observed that the simplified limitation, which is more restrictive, did not present significant differences in relation to the complete limitation strategy that uses the entire capacity of the converter. Being simpler to implement and more restrictive, the simplified strategy could be adopted without significant loss of accuracy.

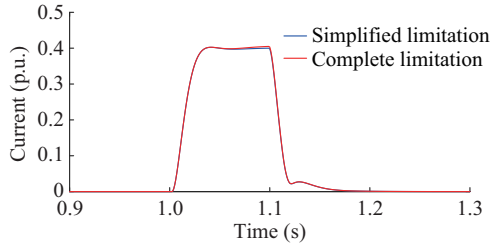

Fig. 15. Negative-sequence current output of generator at bus 1 with simplified and complete current limitation strategies.

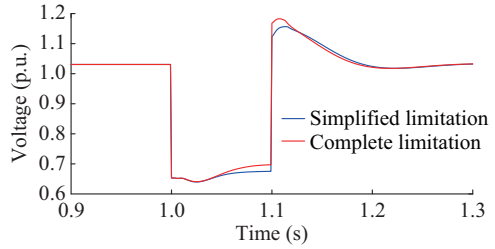

Fig. 16. Positive-sequence voltage at bus 1 with simplified and complete current limitation strategies.

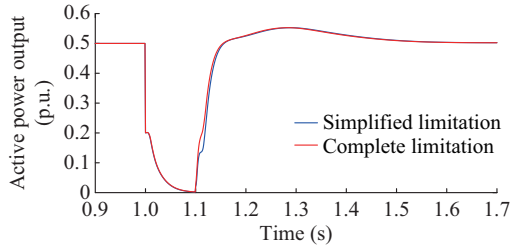

Fig. 17. Active power output of generator at bus 1 with simplified and complete current limitation strategies.

B. BIPS Area

The second test system represents a small area of the BIPS, mostly composed by a 230 kV network, as shown in Fig. 18, and also utilized in [18]. At the interface buses (SE4, SE5, and SE6) of the studied area with the rest of the BIPS, we build the dynamic equivalent model represented by three-phase classical SG models [23], [24]. The studied area contains a thermal power plant connected at SE7 with five generating units, called Willian Arjona (WA). Three cases are created, where the first considers WA with its original SG data, the second considers WA as a CIG PV plant with the same capacity of the thermal plant considered in the first case, with the negative-sequence current suppression, and the third considers the same PV plant as in the second case, but with injection of negative-sequence currents with K_{neg} = 2.5. The current priority is NQP with the simplified limitation strategy. We remark that in order to clearly evaluate and compare the negative-sequence quantities in the three cases, we increase the negative-sequence impedances of the interface equivalent machines.

The distance protection of TL SE2-SE3 employs a three-zone scheme with a quadrilateral characteristic, using the ANSI 67Q function to supervise the ANSI 21 function, as shown in Fig. 7.

1) Single-phase-to-ground Short Circuit

In the first simulation, a 100 ms single-phase-to-ground fault is applied in phase A in the middle of TL SE2-SE3, as shown in Fig. 18. Figure 19 shows the negative-sequence current of WA. We remark that, in the case of CIG with negative-sequence current suppression, there is no negative-sequence currents.

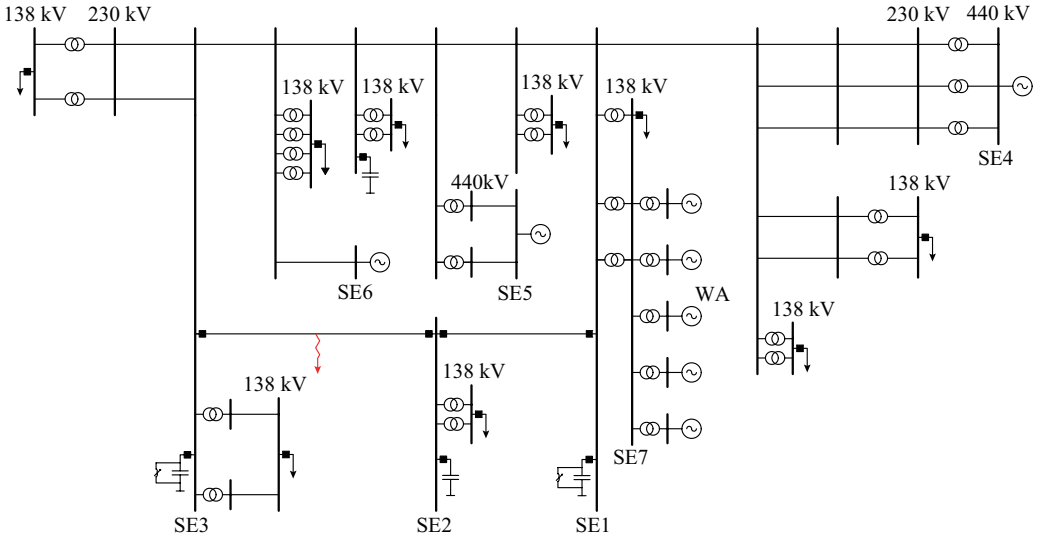

Fig. 18. One-line diagram of part of BIPS.

Figure 20 shows the negative-sequence voltage at the terminal bus of WA. Without the injection of negative-sequence currents, large values of negative-sequence voltages occur during the fault. Figure 21 shows the angular difference between negative-sequence currents and voltages of the TL SE2-SE3 at the SE2 side. It is observed that, with the negative-sequence current suppression, the angular difference of current and voltage at the SE2 side is about 197°, which means that the voltage is leading the current and the relay would not operate because the ANSI 67Q function declares a reverse fault.

At the SE3 side, the relay operates in all three cases, as

shown in Fig. 22. However, at the SE2 side, as observed in Fig. 21, when the ANSI 67Q function is blocked due to the unfavorable angular relationship between negative-sequence quantities, the relay would not operate with the negative-sequence current suppression, but would operate with the injection of reactive negative-sequence currents during the TL fault, as summarized in Table III.

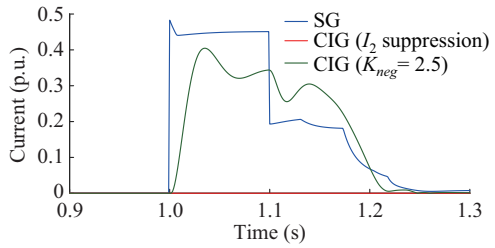

Fig. 19. Negative-sequence current of WA under single-phase-to-ground short circuit.

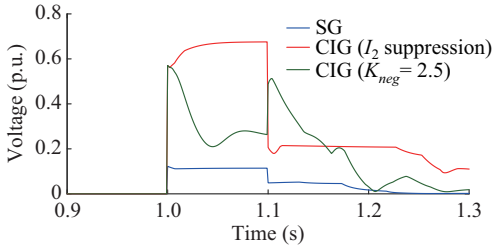

Fig. 20. Negative-sequence voltage at terminal bus of WA under single-phase-to-ground short circuit.

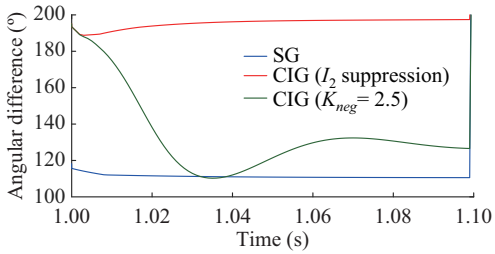

Fig. 21. Angular difference between negative-sequence current and voltage on TL SE2-SE3 (SE2 side) under single-phase-to-ground short circuit.

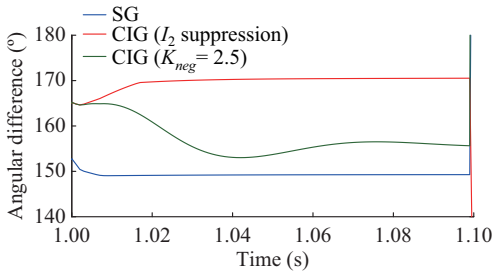

Fig. 22. Angular difference between negative-sequence current and voltage on TL SE2-SE3 (SE3 side) under single-phase-to-ground short circuit.

2) Two-phase-to-ground Short Circuit

In the second simulation with the BIPS system, a 100 ms two-phase-to-ground fault is applied in phase BC of TL SE2-SE3, also in the middle of the TL as shown in Fig. 18. Figure 23 shows the negative-sequence current of WA.

TABLE III
RELAY OPERATION OF TL SE2-SE3 AT SE2 SIDE UNDER SINGLE-PHASE-TO-GROUND SHORT CIRCUIT

Case	ANSI 21	Directionality of ANSI 67Q
SG	Sensitized	Forward
CIG (I_2 suppression)	Sensitized	Reverse
CIG (K_{neg} = 2.5)	Sensitized	Forward

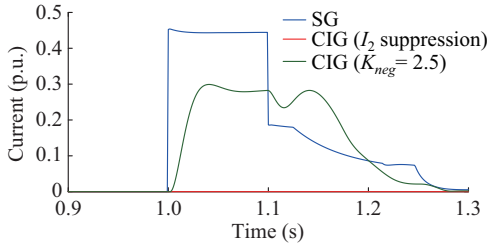

Fig. 23. Negative-sequence current of WA under two-phase-to-ground fault.

In this case, the injected negative-sequence current is smaller than that in the single-phase-to-ground short-circuit case, because the negative-sequence voltages are smaller than the previous case, as shown in Fig. 24.

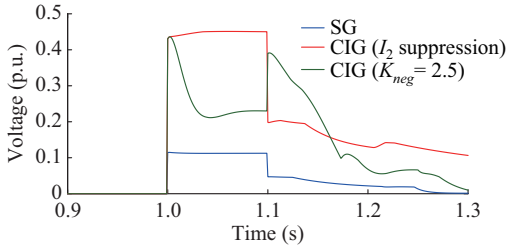

Fig. 24. Negative-sequence voltage of WA under two-phase-to-ground fault.

Figures 25 and 26 show the angular difference between negative-sequence current and voltage of TL SE2-SE3 at SE2 side and at SE3 side, respectively. The injected negative-sequence reactive currents reduce the discrepancy in the angular difference of the negative-sequence quantities. Without the negative-sequence current injection, ANSI 67Q blocks relay operation at SE2 due to unfavorable angular relationship (about 195° of angular difference). With negative-sequence current injection, the relay would operate, as shown in Table IV. Similar to the single-phase-to-ground short-circuit case, the relay located at SE3 is less sensitive to the injected negative-sequence of the CIG at WA.

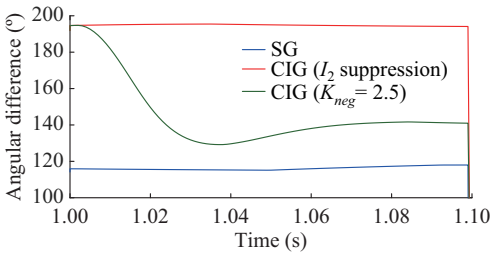

Fig. 25. Angular difference between negative-sequence current and voltage of TL SE2-SE3 (SE2 side) under two-phase-to-ground fault.

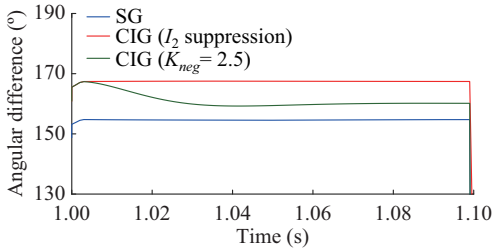

Fig. 26. Angular difference between negative-sequence current and voltage of TL SE2-SE3 (SE3 side) under two-phase-to-ground fault.

TABLE IV
RELAY OPERATION OF TL SE2-SE3 AT SE2 SIDE UNDER TWO-PHASE-TO-GROUND SHORT CIRCUIT

Case	ANSI 21	Directionality of ANSI 67Q
SG	Sensitized	Forward
CIG (I_2 suppression)	Sensitized	Reverse
CIG (K_{neg} = 2.5)	Sensitized	Forward

VI. CONCLUSION

This paper presents an asymmetric current injection controller model for CIGs to be used in fundamental-frequency three-phase RMS dynamic simulation tools.

The system representation in the three-phase RMS dynamic framework allows: ① an adequate approximate representation of asymmetric current injection controller for CIG; ② an interconnection-wide representation of the protection in stability simulations; ③ a more realistic representation of unbalanced faults; ④ the integration of protecting relays involved in phase and ground circuitry; ⑤ a much faster simulation than EMT simulation, particularly considering large- to medium-size systems.

This paper also presents a simplified current limitation strategy and a complete current limitation strategy with various priority sequences of the negative-, active positive-, and reactive positive-sequence currents.

Simulation results in two test systems show the effectiveness of the proposed controller in the assertiveness of negative-sequence directional elements in distance relays.

REFERENCES

[1] IEEE PES, "Impact of inverter based generation on bulk power system dynamics and short-circuit performance," Technical Report PES-TR68, Sept. 2018.
[2] IEEE PES, "System neutral grounding considerations for inverter-interfaced distributed energy resources," Technical Report PES-TR21, Sept. 2018.
[3] *IEEE Guide for Protective Relay Applications to Transmission Lines*, IEEE Standard C37.113-2015, 2016.
[4] P. M. Anderson, *Power System Protection.* New York: IEEE Press, 1999, pp. 377-572.
[5] J. L. Blackburn and T. J. Domin, *Protective Relaying – Principles and Aplications*. 4th ed., Broken: CRC Press, 2007, pp. 411-510.
[6] F. Calero, "Rebirth of negative-sequence quantities in protective relaying with microprocessor-based relays," in *Proceedings of 58th Annual Conference for Protective Relay Engineers*, College Station, United States, Mar. 2004, pp. 190-219.
[7] R. Teodorescu, M. Liserre, and P. Rodríguez, *Grid Converters for Photovoltaic and Wind Power Systems*. New York: IEEE Wiley Press, 2010, pp. 237-354.
[8] IEEE PES, "Protection challenges and practices for interconnecting inverter based resources to utility transmission systems," Technical Report PES-TR81, Jul. 2020.
[9] M. Nagpal and C. Henville, "Impact of power-electronic sources on transmission line ground fault protection," *IEEE Transactions on Power Delivery*, vol. 33, no. 1, pp. 62-70, Feb. 2018.
[10] A. S. Chen, A. Shrestha, F. A. Ituzaro *et al*., "Addressing protection challenges associated with type 3 and type 4 wind turbine generators," in *Proceedings of 68th Annual Conference for Protective Relay Engineers*, College Station, United States, Mar. 2015, pp. 335-344.
[11] A. Haddadi, I. Kocar, and E. Farantatos, "Impact of inverter-based resources on protection schemes based on negative sequence components," *IEEE Transactions on Power Delivery*, vol. 36, no. 1, Mar. 2020, pp. 289-298.
[12] A. Haddadi, I. Kocar, J. Mahseredjian *et al*., "Negative sequence quantities-based protection under inverter-based resources – challenges and impact of the German grid code", in *Proceedings of 21st Power Systems Computation Conference*, Porto, Portugal, Jun. 2020, pp. 1-12.
[13] T. Neumann, T. Wijnhoven, G. Deconinck *et al*., "Enhanced dynamic voltage control of type 4 wind turbines during unbalanced grid faults," *IEEE Transactions on Energy Conversion*, vol. 30, no. 4, pp. 1650-1659, Dec. 2015.
[14] I. Erlich, T. Neumann, F. Shewarega *et al*., "Wind turbine negative sequence current control and its effect on power system protection," in *Proceedings of 2013 IEEE PES General Meeting*, Vancouver, Canada, Jul. 2013, pp. 1-5.
[15] G. Kou, J. Jordan, B. Cockerham *et al*., "Negative-sequence current injection of transmission solar farms," *IEEE Transactions on Power Delivery*, vol. 35, no. 6, pp. 2740-2743, Dec. 2020.
[16] T. Wijnhoven, G. Deconinck, T. Neumann *et al*., "Control aspects of the dynamic negative sequence current injection of type 4 wind turbines," in *Proceedings of 2014 IEEE PES General Meeting|Conference & Exposition*, National Harbor, USA, Jul. 2014, pp. 1-5.
[17] *Technical Connection Rules for Extra-High Voltage,* VDE FNN VDE-AR-N 4130, 2018.
[18] G. N. Taranto, T. M. L. Assis, and J. M. T. Marinho, "Integrating relay models in three-phase RMS dynamic simulation," *IEEE Transactions on Power Systems*, vol. 36, no. 5, pp. 4551-4561, Sept. 2021.
[19] WECC Renewable Energy Modeling Task Force, "WECC Wind Power Plant Dynamic Modeling Guide," Apr. 2014, USA.
[20] WECC Renewable Energy Modeling Task Force, "WECC PV Power Plant Dynamic Modeling Guide", Apr. 2014, USA.
[21] G. N. Taranto and J. M. T. Marinho, "Simulation of integrated transmission and distribution networks with a hybrid three-phase/single-phase formulation," in *Proceedings* of *Bulk Power System Dynamics and Control X, IREP Symposium*, Espinho, Portugal, Aug. 2017, pp. 1-7.
[22] S. Chou, C. Lee, P. Cheng *et al*., "A reactive current injection technique for renewable energy converters in low voltage ride-through operations," in *Proceedings of 2011 IEEE PES General Meeting*, Detroit, USA, Jul. 2011, pp. 1-7.
[23] P. Kundur, *Power System Stability and Control*. New York: McGraw-Hill, 1994.
[24] E. B. Makran, V. O. Zambrano, R. G. Harley *et al*., "Three-phase modeling for transient stability of large scale unbalanced distribution systems," *IEEE Transactions on Power Systems*, vol. 4, no. 2, pp. 487-493, May 1989.

Victor A. F. Almeida received the B. Sc. degree in electrical engineering from Federal University of Rio de Janeiro, Rio de Janeiro, Brazil, in 2019. He is currently pursuing his M. Sc. degree in electrical engineering from Federal University of Rio de Janeiro. He is currently a Researcher at Electrical Engineering Department of the Federal University of Rio de Janeiro (COPPE/UFRJ), Rio de Janeiro, Brazil. His research interests include dynamics, control and protection of power systems and renewable energy resources.

Glauco N. Taranto received the B.Sc. degree from the State University of Rio de Janeiro, Rio de Janeiro, Brazil, in 1988, M.Sc. degree from the Pontifical Catholic University, Rio de Janeiro, Brazil, in 1991, and Ph.D. degree from Rensselaer Polytechnic Institute, Troy, NY, USA, in 1994, all in electrical engineering. In 2006, he was a Visiting Fellow in Centro Elettrotecnico Sperimentale Italiano (CESI), Milan, Italy. He is a Professor of Electrical Engineering at Electrical Engineering Department of the Federal University of Rio de Janeiro (COPPE/FURJ), Rio de Janeiro, Brazil, where he works since 1995. He is the Chair of the Power System Stability Subcommittee of the

IEEE PES Power System Dynamic Performance Technical Committee (2019-2022), and the Chair of the ongoing Task Force on "Integrating relay models with RMS dynamic simulation". He was Editor of the IEEE Transactions on Power Systems (2016-2020). His research interests include power system dynamics, protection and control.

José M. T. Marinho received his B. Sc. degree in electrical engineering from the Federal University of Juiz de Fora, Juiz de Fora, Brazil, in 1990, the M.Sc. and D.Sc. degrees in electrical engineering from the Federal University of Rio de Janeiro, Rio de Janeiro, Brazil, in 1998 and 2008, respectively. He is a Master Engineer in Petrobras S. A., Rio de Janeiro, Brazil. His research interests include computational modeling and applications in power and industrial systems.